Generalized model for laser-induced surface structure in metallic glass*

Lin-Mao Ye(叶林茂)[1], Zhen-Wei Wu(武振伟)[1,2], Kai-Xin Liu(刘凯欣)[1,2,†], Xiu-Zhang Tang(汤秀章)[3], and Xiang-Ming Xiong (熊向明)[1]

[1] *LTCS and Department of Mechanics & Engineering Science, College of Engineering, Peking University, Beijing* 100871, *China*
[2] *Center for Applied Physics and Technology, Peking University, Beijing* 100871, *China*
[3] *China Institute of Atomic Energy, Beijing* 102413, *China*

(Received 17 December 2015; revised manuscript received 23 February 2016; published online 20 April 2016)

The details of the special three-dimensional micro-nano scale ripples with a period of hundreds of microns on the surfaces of a Zr-based and a La-based metallic glass irradiated separately by single laser pulse are investigated. We use the small-amplitude capillary wave theory to unveil the ripple formation mechanism through considering each of the molten metallic glasses as an incompressible viscous fluid. A generalized model is presented to describe the special morphology, which fits the experimental result well. It is also revealed that the viscosity brings about the biggest effect on the monotone decreasing nature of the amplitude and the wavelength of the surface ripples. The greater the viscosity is, the shorter the amplitude and the wavelength are.

Keywords: metallic glasses, pulse laser processing, micro-nano scale surface structure, viscosity

PACS: 81.16.Rf, 81.05.Kf, 66.20.Cy, 81.15.Fg **DOI:** 10.1088/1674-1056/25/6/068104

1. Introduction

Laser-induced periodic surface structures (LIPSSs) for various materials, such as metals and semiconductors, have been well studied[1–6] by the scientific and engineering community since laser operating devices were invented. Some unique micro-nano scale surface structure irradiated by laser has also been discovered. As the fabrication of the micro-nano scale surface structure has been well used in many fields,[7–12] the morphological formation mechanism of the structure has attracted a great deal of attention.[13–16] Based on previous researches, the fluence of the laser is considered as one of the major factors for the formation of LIPSSs, which mainly affects the generated surface electromagnetic wave or the capillary wave on the surface.[1,13] However, there are different structures appearing on the surface for various materials under the same laser condition. The properties of the material should also be an important factor for the formation mechanism, which is less discussed.

Bulk metallic glass (BMG) with excellent features[17,18] like high strength, good magnetic properties and corrosion resistance processed by pulse laser has a more complex surface phenomenon than many other materials. As described in our previous work,[14] there are especially novel concentric rippling wave structures on the surface of BMG irradiated by pulse laser. The wavelength and the amplitude decreased from the inside to the outside. Liu *et al.*[15] gave a model to predict the characteristic interval of the ripples via perturbation analysis. However, there are no unified models for the whole ripple structures and few investigations into the effect of material properties on the morphological formation mechanism. Making clear the special surface structural evolution of BMGs induced by single laser and the effect of the properties of BMGs will be helpful for understanding the BMGs in physics and materials science, which show a series of improved features, interesting phenomenon, and practical applications.

In this work, the three-dimensional (3D) surface morphologies of a Zr-based and a La-based metallic glass irradiated separately by nano-second single pulse laser are scanned by atomic force microscopy (AFM). Based on the experimental result, we give a generalized theoretical model for describing the surface morphology of the BMG irradiated by laser, which is based on the hydrodynamics of a small-amplitude capillary wave propagating in deep water by considering BMG as an incompressible and high viscosity fluid. The experimental results agree with the results from our model very well. It is also revealed that the high viscosity of BMG is more important for forming the special ripples than the different experimental results of the two kinds of materials.

2. Experimental details

As described in our previous work,[14] two kinds of special BMGs $Zr_{55}Cu_{30}Al_{10}Ni_5$ (at.%) and $La_{55}Ni_{20}Al_{25}$ (at.%) were prepared by the arc melting and drop-casing method, and cut into cylindrical targets, each with diameter 5 mm and

*Project supported by the National Natural Science Foundation of China (Grant Nos. 10572002, 10732010, and 11332002).
†Corresponding author. E-mail: kliu@pku.edu.cn
© 2016 Chinese Physical Society and IOP Publishing Ltd

height 5 mm, by wire electrode cutting. The specimen surfaces were polished until the roughness was less than 30 nm. The amorphous material nature was also confirmed by x-ray diffraction (XRD) as well as differential scanning calorimetry (DSC) with a heating rate of 20 K/min. Then, a single pulse Nd: YAG solid state laser with wavelength 532 nm, pulse width 10 ns and the maximum energy 1 J was used to irradiate the polished target surface at room temperature. After irradiation, another XRD experiment was performed to test the amorphous nature, and the two-dimensional (2D) and 3D surface morphology were observed by scanning electron microscopy (S-4800) and atomic force microscopy Dimension ICON, respectively.

3. Results and discussion

Figure 1(a) displays the whole 2D surface features of the Zr-based BMG irradiated by single pulse laser with a peak incidence of about 5.5×10^{12} W/m^2. Figure 1(b) shows the details of the magnified ripples marked by "A" in Fig. 1(a). As shown in Figs. 1(a) and 1(b), there are concentric ripples on the edge of the irradiated area of the Zr-based BMGs. The characteristic widths of the ripples are not constant, whose values range from 4 μm to 1 μm, become smaller from the inside to the outside, which is different from the scenarios of the other materials such as epoxy resin and some metals. Figures 1(c) and 1(d) show the experimental results of La-based BMG under the same condition. There are also concentric ripples with varying characteristic width. However, their amplitudes and wavelengths are larger than those of the Zr-based BMGs.

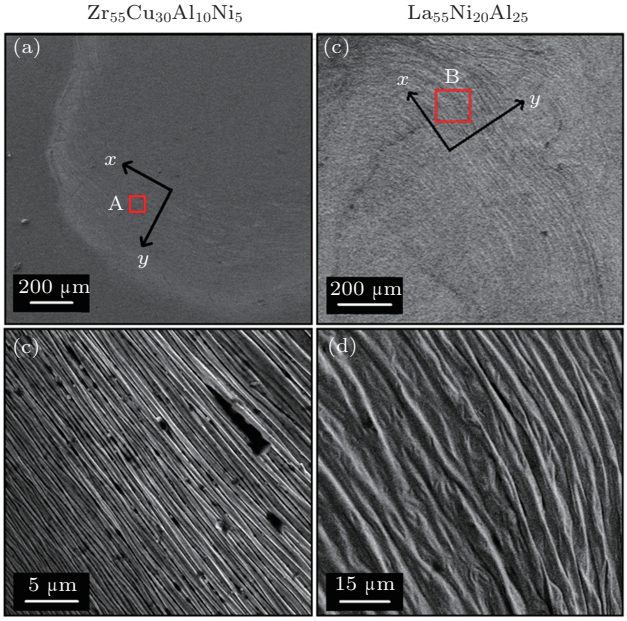


Fig. 1. (color online) Micrographs of the surface morphology of $Zr_{55}Cu_{30}Al_{10}Ni_5$ ((a) and (b)) and $La_{55}Ni_{20}Al_{25}$ ((c) and (d)) irradiated by a single pulse laser with an intensity of about 5.5×10^{12} W/m^2. Panels (a) and (c) show the entire SEM view of the irradiated area, panel (b) displays the close-up view of the area "A" marked in panel (a), and panel (d) exhibits the close-up view of the area "B" marked in panel (c).

The values of the wavelength change from 10 μm inside to 1 μm outside. The later XRD experimental results show that the material still holds the amorphous characteristic.

In order to make further study on the formation of the special surface patterns, detailed AFM observations of the ripple structure are shown in Fig. 2. Figures 2(a) and 2(b) show the 2D morphologies for the middle parts of the ripples. Figures 2(c) and 2(d) display the 3D morphologies corresponding to Figs. 2(a) and 2(b), respectively. Then we obtain the corresponding statistical characteristic wavelengths and amplitudes of the ripples by analyzing the values of the data along the selected parallel lines in the wave propagating direction every few micrometers in the 3D figures (example is shown as red lines in Figs. 2(a) and 2(b)). Based on the experimental results, a generalized model is presented to describe the special morphology on the surface.

The statistical experimental and the analytical fitting results for the amplitude, the wavelength and the whole ripples are all shown in Figs. 3. The values of the wavelength and the amplitude are significantly different between the two kinds of materials. As the laser condition is the same, it can be inferred that the results depended on the properties of the material.

When BMGs are irradiated by the single high energy laser, its surface in the radiated zone absorbs large amounts of energy, which leads to the temperature rising up to glass transition temperature in a very thin layer. The intensity of the laser conforms to spatial Gaussian distribution, which can be given as[19]

$$I(r,\tau) = I_0(\tau)\exp\left(-r^2/2R_0^2\right), \tag{1}$$

where $I_0(\tau)$ is the laser peak intensity at time τ, r is the distance from the center, and R_0 is a radius parameter. According to the heat conductivity equation and Eq. (1), the temperature on the surface can be expressed as[2,20]

$$T(r,\tau) = 2\alpha I_0(\tau)(\tau/\pi K\rho c)^{1/2}\exp\left(-r^2/2R_0^2\right) + T_a, \tag{2}$$

where α is the effective optical absorption of the material, K is the thermal conductivity, ρ is the density, c is the heat capacity, and T_a is the ambient temperature. The energy in the center is higher, which causes the temperature to rise up to the melting point. During the irradiation, there will be pressure[21,22] caused by the laser, which mainly affects the central area of the melting BMGs and produces a shock wave propagating outwards in the molten layer. It induces the morphology of the recessed flat shape in the center and the wave form on the edge. The whole process is much more complex including melting, flowing and solidifying. We mainly discuss the wave propagating process, which contributes most to the formation of the special ripple pattern on the surface of the BMGs.

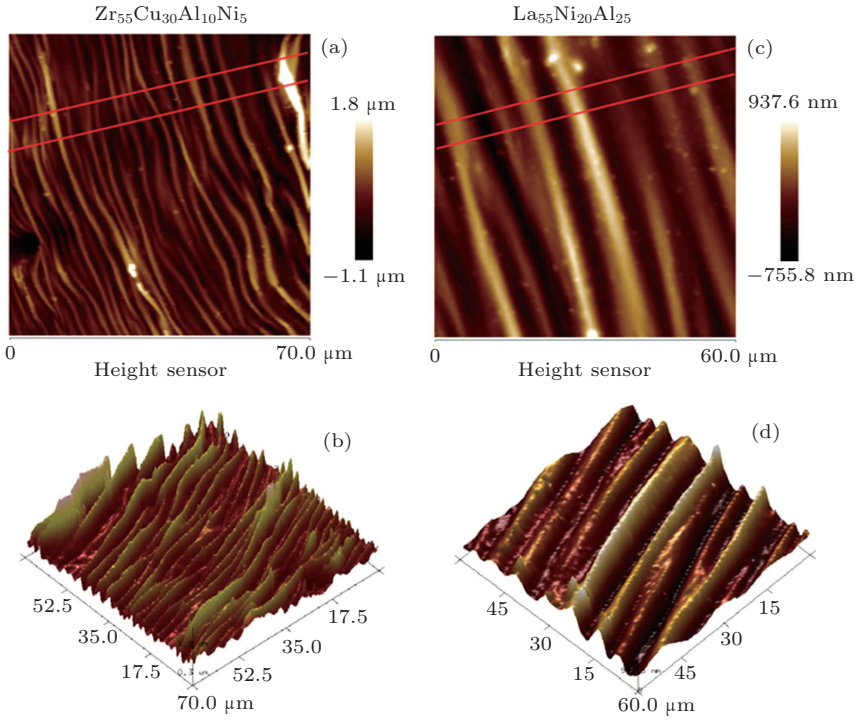


Fig. 2. (color online) AFM images for $Zr_{55}Cu_{30}Al_{10}Ni_5$ ((a) and (b)) and $La_{55}Ni_{20}Al_{25}$ ((c) and (d)). Panels (a) and (c) show the 2D details near the middle part of the ripples, and panels (b) and (d) display the 3D details corresponding to panels (a) and (c), respectively.

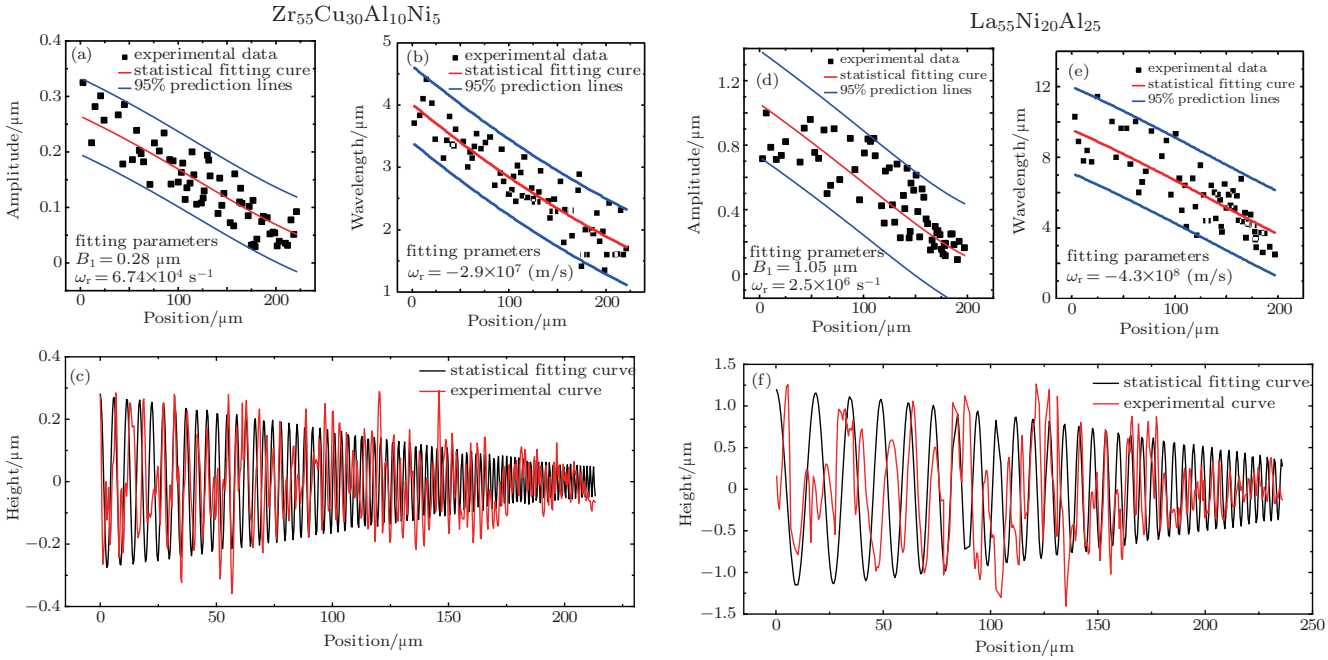


Fig. 3. (color online) Experimental data and the theoretical statistical data along the x direction of the wave such as the red exemplificative lines shown in Figs. 2(a) and 2(c). Panels (a) and (d) show the position-dependent amplitudes, panels (b) and (e) the position-dependent wavelengths, and panels (c) and (f) are the position-dependent entire cures. Panels (a), (b), and (c) refer to the results of $Zr_{55}Cu_{30}Al_{10}Ni_5$, and panels (d), (e), and (f) show the results of $La_{55}Ni_{20}Al_{25}$. In panels (a), (b), (d), and (e), the grid points are the experimental statistical data, the red line is the theoretical fitting curve, and the fitting parameters are given. The blue lines are the 95% prediction lines, which means that the probability for true values of the experimental data falling into the intervals is 95%. Panels 3(c) and 3(f) show the comparison between whole waves, i.e. between the statistical fitting curve (black) drawn from Eq. (10) and the experimental curve (red).

As the amplitude attenuates rapidly and nearly disappears on the edge observed in Fig. 3, it can be assumed that there is no reflection in the wave propagating process. In other words, the wave in the molten pool has not reached the boundary before the molten BMGs freeze down. The statistical analysis shown in Fig. 3 presented that the magnitudes of the characteristic wavelength and the amplitude are on the order of 10^{-6} m and 10^{-7} m for the Zr-based BMGs and 10^{-5} m and 10^{-6} m for the La-based BMGs, respectively. It can be considered as $h \ll \lambda$. So the whole process can be assumed to be a small-amplitude capillary surface wave propagating in the infinite supercooled metallic glass liquid pool without reflection

before the melting BMGs freeze down. As the laser is a circularly polarized laser and the ripples as shown in Fig. 1 are approximately axisymmetric, the amplitude and the wavelength can be considered to be the same as those in the circumferential orientation. Then the 3D problem can be simplified into a 2D problem and the velocity vector of the particles v can be expressed as (u,w).

As shown in previous experimental studies,[23–26] the viscosity of the melting BMGs alloys is very large. In our experiment, the magnitudes of the following characteristic coefficients are $\mu > 10^{-1}$ Pa·s,[20] $\sigma_0 \sim 100$ N/m,[13] and $g \sim 10^1$ m/s^2, so there is $\left|\mu\nabla^2 v\right| \gg \left|\sigma_0 \partial^2 v/\partial x^2\right| \gg |g|$, where μ is the viscosity coefficient, σ_0 is the surface tension coefficient, and g is the acceleration vector of gravity. The viscosity can be considered as a main reason for forming the surface morphology. As there are more than a hundred cycles and the amplitude and the wavelength of the surface ripples are very small and almost unchanged in several adjacent cycles, we can assume that the viscosity and surface tension coefficient to be constant in each cycle. In other words, the conditions in each cycle can be regarded as being constant. In the following, we solve the problem for each cycle. According to the hydrodynamics theory, there are the approximate conditions $|v| \sim h/C$, $|\partial v/\partial t| \sim h/C^2$, and $|(v\cdot\nabla)v| \sim h^2/\lambda C^2$ (C, h, and λ are the period, amplitude and wavelength of the wave, respectively) for small-amplitude capillary surface wave in the deep liquid.[27,28] The external force term, the nonlinear speed term and the gravity term can be ignored in comparison with the linear and the surface tensor ones. Then the governing equations can be given with the original point defined on the edge of the irradiation central area, which is the starting point of the ripples. The x axis is along the wave propagating direction on the surface, and the z axis is downwards perpendicular to the x axis. The molten BMGs are regarded as being an incompressible and viscous fluid. The governing equations in each independent cycle can be simply given in Euler coordinates as

$$\begin{cases} \rho\partial u/\partial t = -\partial P/\partial x + \mu\left(\partial^2 u/\partial x^2 + \partial^2 u/\partial z^2\right), \\ \rho\partial w/\partial t = -\partial P/\partial z - g + \mu\left(\partial^2 w/\partial x^2 + \partial^2 w/\partial z^2\right), \\ \partial u/\partial x + \partial w/\partial z = 0, \\ \mathrm{d}\rho/\mathrm{d}t = 0. \end{cases} \tag{3}$$

The boundary condition on the surface ($z = 0$) can be shown as

$$\begin{cases} w \approx \partial\xi/\partial t, \\ \sigma_{xy} = \mu\left(\partial u/\partial u + \partial w/\partial x\right) = 0, \\ \sigma_{yy} = -P + 2\mu\partial w/\partial z = -P_0 + \sigma_0\partial^2\xi/\partial x^2, \end{cases} \tag{4}$$

where $y = \xi(x,t)$ is the interface function after perturbation, and P_0 is the pressure above the surface, which can be considered to be fixed along with x in each independent cycle. Considering $w_1(z) \to 0$ when $z \to -\infty$, the solution of Eqs. (3) and (4) can be expressed as

$$\begin{cases} u = \left(A\mathrm{e}^{kz} + B\mathrm{e}^{bz}\right)\mathrm{e}^{\mathrm{i}(kx-\omega t)}, \\ w = \left(-A\mathrm{e}^{kz}i - B\mathrm{e}^{bz}ki/b\right)\mathrm{e}^{\mathrm{i}(kx-\omega t)}, \\ P/\rho = P_0/\rho - gz + A\mathrm{e}^{kz}\mathrm{e}^{\mathrm{i}(kx-\omega t)}\omega/k, \end{cases} \tag{5}$$

where k and ω are the complex numbers, A, B, and $b = \sqrt{k^2 - \mathrm{i}\omega/w}$ (Re $b > 0$) are the parameters. Inserting Eq. (5) into Eq. (4), considering $w|_{z=0} \approx \partial\xi/\partial t = (-\mathrm{i}A - \mathrm{i}k\gamma_2 B/b)\mathrm{e}^{\mathrm{i}(kx-\omega t)}$, $\xi \approx 0$, and $k^2\sigma_0/\rho \gg g$, and ignoring the quadratic term of A and B, we have

$$\begin{cases} 2kbA + \left(k^2 + b^2\right)B = 0, \\ \left(k^2\sigma_0/\rho - \omega^2/k - 2\mathrm{i}kw\omega\right)A \\ \quad + \left(k^3\sigma_0/\rho b - 2\mathrm{i}kw\omega\right)B = 0. \end{cases} \tag{6}$$

As equation (6) has the nontrivial solution, the coefficient matrix determinant is zero, and there is

$$(b^2 + k^2)\omega^2/k + 2\mathrm{i}k\mu\omega(b-k)^2/\rho + \mathrm{i}\omega k^2\sigma_0/\mu = 0. \tag{7}$$

Assuming that $\rho\omega/k^2\mu \ll 1$, there is $b \sim k$ and k can be approximately given as

$$k = k_r + \mathrm{i}k_i = 2\mathrm{i}\omega\mu/\sigma_0 = 2\mathrm{i}(\omega_r + \mathrm{i}\omega_i)\mu/\sigma_0, \tag{8}$$

where $k_r = 2\pi/\lambda$ is the wavenumber, $\omega_r = 2\pi/C$ is the circular frequency, and k_i and ω_i are the corresponding time and spatial attenuations, respectively. Considering that $\partial\xi/\partial t \approx w|_{z=0} = (-\mathrm{i}A - \mathrm{i}Bk/b)\mathrm{e}^{\mathrm{i}(kx-\omega t)}$, the interface morphology function in each independent circle can be expressed as

$$\xi = (A/\omega + kB/b\omega)\mathrm{e}^{\mathrm{i}(kx-\omega t)}. \tag{9}$$

While referring to the whole rippling morphology on the surface, neither the amplitude nor the wavelength of the wave in spatial scale is constant but decreases gradually from the inside to the outside, which is mainly caused by the temperature-dependent viscosity. We assume that the time scale for the solution is constant as τ_0 and the variable viscosity coefficient on the surface, changes only in the x direction, which is defined as $\mu(x)$. Then the circular frequency ω_r and the corresponding time attenuation ω_i, which are both parameters of time scale, can also be regarded as being constant when the sample solidifies. Inserting Eq. (8) into Eq. (9) and considering $t = \tau_0$ and $b \sim k$, we obtain the formula of the ripples on the surface

$$\xi_r(\mu) = a(\mu)\cos\left(2\pi x/\lambda(\mu) - \phi_0(\mu)\right). \tag{10}$$

The amplitude and the wavelength of the surface ripples can be expressed as

$$a(x) = a(\mu) = B_1\exp\left(-2x\omega_r\mu(x)/\sigma_0\right),$$

and

$$\lambda(x) = \lambda(\mu) = 2\pi/k_r = -\pi\sigma_0/\omega_i\mu(x), \tag{11}$$

where $B_1 = \left|\omega^{-1}\right||A+B|\exp(\omega_i\tau_0)$ is an undetermined parameter, $a(\mu)$, $\lambda(\mu)$, and $\varphi_0(\mu)$ are the amplitude, the wavelength, and the phase separation of the wave, which depend on the viscosity.

The viscosity depends on the temperature T and obeys the Vogel–Fulcher–Tammann (VFT) relationship.[23–26] It is expressed as $\mu = \mu_0\exp(A_0/(T-T_1))$, where μ_0, A_0, and T_1 are three VFT constants. It can be assumed that the time scale in Eq. (2) is the constant denoted as τ_0 and the viscosity coefficient on the surface changes only in the x direction. Inserting Eq. (2) into the VFT relationship, the viscosity on the surface can be expressed approximately as

$$\mu(x) = \mu_0\exp\left(\frac{A_0}{(T_0-T_a)\exp(-(r_0+x)^2/R_0^2)+T_a-T_1}\right), \tag{12}$$

where $T_0 = T(0,\tau_0) = 2\alpha(\tau_0/\pi K\rho c)^{1/2}I_0(\tau_0)+T_a$ is the temperature at the central point on the surface at time τ_0. All the parameters can be measured experimentally. Equations (10)–(11) fully describe the surface ripple patterns.

Referring to earlier work[14,15,21–26,29] and our experimental data, one could use $T_a \approx 300$ K, $\alpha \approx 0.1$, $\tau_0 = 1\times10^{-8}$ s, $r_0 \approx 1.0\times10^{-3}$ m, $R_0 \approx 1.25\times10^{-3}$ m, $I_0(\tau_0) \approx 5.5\times10^{12}$ W/m^2, $\rho_{Zr} \approx 6400$ kg/m^3, $c_{Zr} \approx 1200$ J/(kg·K), $\sigma_{0Zr} \approx 0.85$ N/m, $K_{Zr} \approx 100$ W/(m·K), $A_{0Zr} \approx 8531$ K, $\mu_{0Zr} \approx 9.36\times10^{-5}$ Pa·s, and $T_{1Zr} \approx 383.1$ K for Zr-based BMG for the simulation, with ignoring the temperature effect on the parameters as they change little in our experiment. According to the above analysis and fitting the experimental data to Eqs. (10) and (11), the statistical fitting values for the parameters in the formula can be obtained as $B_{1Zr} \approx 2.8\times10^{-7}$ m, $\omega_{rZr} \approx 6.7\times10^4$ s^{-1}, and $\omega_{iZr} \approx -2.9\times10^7$ m/s. For La-based BMG,[21–26,29] there are $\rho_{La} \approx 6140$ kg/m^3, $c_{La} \approx 1100$ J/(kg·K), $\sigma_{0La} \approx 0.5$ N/m, $K_{La} \approx 80$ W/(m·K), $\mu_{0La} \approx 2.58\times10^{-5}$ Pa·s, $A_{0La} \approx 5517$ K, and $T_{1La} \approx 306.5$ K, and the other parameters are considered to be the same as those mentioned above. Like the above analysis, the statistical fitting values for the parameters in the formula can be obtained as $B_{1La} \approx 1.05\times10^{-6}$ m, $\omega_{rLa} \approx 2.5\times10^6$ s^{-1}, and $\omega_{iLa} \approx -4.3\times10^8$ m/s. Ignoring the phase separation of the wave, the formulas of the free surface morphology and the viscosity coefficient could be obtained.

The experimental and the statistical fitting results of the ripples on the surface are shown together in Fig. 3(c) for Zr-based BMG and Fig. 3(f) for La-based BMG. Figures 3(c) and 3(f) both clearly show that the whole attenuation trends of the amplitude and the wavelength simulated by Eqs. (10) and (11) are consistent with the experimental data well. While the viscosity force has a great contribution to the formation of the ripples, it can be considered that the viscosity of the metallic glass mainly affects the amplitude and the wavelength. From the inside to the outside, the temperature decreases a lot, causing the viscosity coefficient to rise. Considering the viscosities of the two kinds of BMGs or comparing the inside part with the outside part of one kind of BMG, it can be inferred that the greater the viscosity is, the shorter the amplitude and the wavelength are. It could also be preliminarily concluded that the form of the ripples is determined by the characters of the laser as well as the viscosity of the BMGs.

4. Conclusions and perspectives

In this work, following ns pulse irradiation, a type of dense micro-nano scale ripple pattern with a period of hundreds of microns on the surface is produced. The formulation of the ripples is the result of the small-amplitude capillary wave propagating in an infinite metallic glass forming a supercooled liquid pool. Based on hydrodynamics, a generalized theory can be given to unveil the ripples forming mechanism in metallic glass. In our experiment, the characteristics of monotonically reducing the amplitude and wavelength of the special ripples mainly depend on the high viscosity of the molten BMGs. The greater the viscosity, the smaller the amplitude is and the shorter the wavelength. It can be concluded further that the generation and the features of the special morphology are primarily dependent on the characteristics of laser, material, especially viscosity for BMGs. This research can also help us quantitatively obtain the desired micro and nano surface structures by adjusting the laser parameters and choosing suitable BMGs materials.

Acknowledgment

We are grateful to the State Key Laboratory of Advanced Optical Communication Systems & Networks of Peking University for supplying the equipment of atomic force microscopy dimension ICON.

References

[1] Hwang T Y and Guo C 2012 *Appl. Phys. Lett.* **101** 021901
[2] Xia Y Y, Wang Q P, Mei L M, Tan C Y, Yue S B, Xu B Z and Liu X D 1991 *J. Phys. D: Appl. Phys.* **24** 1933
[3] Hohm S, Herzlieb M, Rosenfeld A, Kruger J and Bonse J 2013 *Appl. Phys. Lett.* **103** 254101
[4] Clark S E and Emmony D C 1989 *Phys. Rev. B* **40** 2031
[5] Cho H, Kim S and Ki H 2012 *Acta Mater.* **60** 6237
[6] Jarmakani H, Maddox B, Wei C T, Kalantar D and Meyers M A 2010 *Acta Mater.* **58** 4604

[7] Zhang J C, Liu Y W, Huang C L, Zhang Q Q, Yi Y, Zeng Y, Zhu X L, Fan Q P, Qian F, Wei L, Wang H B, Wu W D and Cao L F 2014 *Chin. Phys. Lett.* **31** 124204

[8] Liang L X, Deng Y and Wang Y 2013 *Chin. Phys. Lett.* **30** 108104

[9] Li Y G, Yang C S, Liu J Q and Sugiyama S 2011 *Chin. Phys. Lett.* **28** 038101

[10] Wang H P, Ke S Y, Yang J, Wang Y and Yang Y 2014 *Acta Phys. Sin.* **63** 098104 (in Chinese)

[11] Liao Y J, Lou Y H, Wang Z K and Liao L S 2014 *Chin. Phys. B* **23** 118508

[12] Zhao L, Jin Y R, Li J, Deng H and Zheng D N 2014 *Chin. Phys. B* **23** 087402

[13] Hwang T Y and Guo C 2011 *J. Appl. Phys.* **109** 083521

[14] Liu W D, Ye L M and Liu K X 2011 *J. Appl. Phys.* **109** 043109

[15] Liu Y, Jiang M Q, Yang G W, Guan Y J and Dai L H 2011 *Appl. Phys. Lett.* **99** 191902

[16] Lu C, Recht D and Arnold C 2013 *Phys. Rev. Lett.* **111** 105503

[17] Wang W H 2011 *Physics* **40** 703 (in Chinese)

[18] Sun B A and Wang W H 2015 *Prog. Mater Sci.* **74** 211

[19] Vogel A, Noack J, Huettmann G and Paltauf G 2005 *Appl. Phys. B: Lasers Opt.* **81** 1015

[20] Kelly R, Cuomo JJ, Leary P A, Rothenberg J E, Braren B E and Aliotta C F 1985 *Nucl. Instrum. Methods Phys. Res. B* **9** 329

[21] Pirri A N 1977 *Phys. Fluids* **20** 221

[22] Phipps C R, Turner T P, Harrison R F, York G W, Osborne W Z, Anderson G K, Corlis X F, Haynes L C, Steele H S, Spicochi K C and King T R 1998 *J. Appl. Phys.* **64** 1083

[23] Chen H S 1980 *Rep. Prog. Phys.* **43** 353

[24] Busch R, Bake E and Johnson W L 1998 *Acta Mater.* **46** 4725

[25] Yamasaki T, Maeda S, Yokoyama Y, Okai D, FukamiT, Kimura H M and Inoue A 2006 *Intermetallics* **14** 1102

[26] Takeuchi A, Kato H and Inoue A 2010 *Intermetallics* **18** 406

[27] Milne-Thomson L M 1960 *Theoretical Hydrodynamic* (London: Macmillan & Co. Ltd.)

[28] Landau L D and Lifshitz E M 1987 *Fluid Mechanics* (Oxford: Pergamon Press)

[29] Chattopadhyay C, Sangal S andMondal K 2014 *Bull. Mater. Sci.* **37** 83